

Brief communication

Theoretical and experimental study of two-phase flow in micro-channels grooved into horizontal pipes

M.E. Rojas ^{a,*}, M.C. de Andrés ^b

^a *PSA, Energy Department, CIEMAT, Avda. Complutense, 22, 28040 Madrid, Spain*

^b *Renewable Energy Group, Faculty of Physics, U. Complutense, 28040 Madrid, Spain*

Received 20 March 2005; received in revised form 19 January 2006

Keywords: Heat pipes; Grooved micro-channels; Heat transfer enhancement

1. Introduction

In recent decades, the use of heat-transfer-enhancing pipes as a way of improving thermal system efficiency has intensified. Among others, pipes with micro-channels etched in the inner wall are being widely employed in cooling systems and heat pipes – for both air-conditioning and solar thermal collectors – (for example, [Webb, 1994](#)). This type of pipe enhances heat transfer by intensifying convective boiling and/or capillary-driven pumping of liquid in the micro-channels. Due to its great potential, studies on the thermal-hydraulic behaviour of such systems have also increased in recent years. Most of these studies focus on practical considerations, such as the theoretical and/or experimental exploration of heat transfer coefficients for the most frequently used coolants ([Yoshida et al., 1987](#); [Yun et al., 2002](#); [Honda and Wang, 2004](#)). Theoretical studies deal preferentially with closed micro-channels ([Peles et al., 2001](#)), while modelling of two-phase flow in open micro-channels is rather limited. [Peng et al.](#) have investigated the rewetting characteristics of capillary-induced flow in specific cases, such as heated flat horizontal surfaces ([Peng and Peterson, 1991](#)), heated vertical flat plates with a porous coating ([Peng et al., 1992](#)) and heated horizontal pipes with vertical semicircular micro-grooves etched in their inner surface ([Peng et al., 1993](#)).

In the study presented here, [Peng et al.'s model \(1993\)](#) is generalized to any geometry and configuration of micro-channels, being improved with the definitions of dynamic and static liquid front positions. These definitions are quite useful in designing micro-channels for specific applications. The theoretical results are validated with experimental data from pool boiling of water and two carbon steel samples under different saturation conditions.

* Corresponding author. Tel.: +34 91 346 6049; fax: +34 91 346 6037.

E-mail addresses: esther.rojas@ciemat.es (M.E. Rojas), mcandres@fis.ucm.es (M.C. de Andrés).

2. Theoretical study

Let us consider stratified two-phase flow in a horizontal pipe with micro-channels etched in its inner surface (Fig. 1). Even if the bulk flow in the pipe is small, some liquid can rise well above it, flowing in x^* direction, because of capillary pressure in the micro-channels. Then, the portion of the inner surface that is kept wet is improved and the transfer of a heat flux applied externally onto the pipe is enhanced. We look for a theoretical model able to predict the maximum external heat flux that a pipe with open micro-channels is able to withstand while still maintaining efficient heat transfer.

Assuming that thermal behaviour and flow characteristics are the same in all the micro-channels, the analysis of the whole system can be reduced to a thermohydraulic study of just one micro-channel. Although, in principle, it is a problem of two-phase flow, because the liquid flowing in the micro-channel displaces the steam in it, it can be considered single-phase flow if steam-to-liquid resistance is negligible (Dullien, 1992), i.e., if the steam velocity related to the liquid is negligible and the steam pressure is assumed constant in its definition domain (Scheidegger, 1957). This occurs when the two-phase flow inside the microgrooved pipe is stratified. Therefore, the flow behaviour in the micro-channel is given only by the momentum balance equation for the liquid film in the direction of interest, i.e., in the direction defined by u_{x^*} (Fig. 1). Following the approach of Peng et al. (1993), the liquid front velocity is obtained first with no heat flux (adiabatic model). Below this velocity is modified for cases when heat flux is applied.

2.1. Adiabatic model

When no heat flux is applied, and taking the liquid layer in an open micro-channel as the control volume, the balance of forces is

$$(\text{inertial forces}) = (\text{gravitational forces}) + (\text{capillary driving forces}) + (\text{viscous forces}). \tag{1}$$

Taking into account that the liquid layer has a mass m_l , which flows in the x^* direction (defined by the unitary vector u_{x^*} ; Fig. 1) with a liquid front velocity, v_l , the above equation leads to the following expression (Rojas, 2003):

$$\frac{dv_l}{d\theta} = \frac{1}{\rho_l \theta v_l} \left(\frac{2\sigma \cos \beta}{r_c} - \rho_l g R (1 - \cos \theta) \cos \gamma - \mu_l \frac{v_l}{r_H} \frac{A_{cont}}{A_l} - v_l^2 \rho_l \right), \tag{2}$$

where θ is the angular liquid front position; ρ_l and μ_l are the density and dynamic viscosity of liquid, respectively; σ is the surface tension; β is the contact angle of the liquid–steam–solid interface (Fig. 1(b)); r_c is the effective or equivalent capillary radius in the direction of interest; g is the gravitational acceleration; R is the inner radius of the pipe; γ is the micro-channel angle to the vertical (Fig. 1(b)); r_H is the hydraulic radius

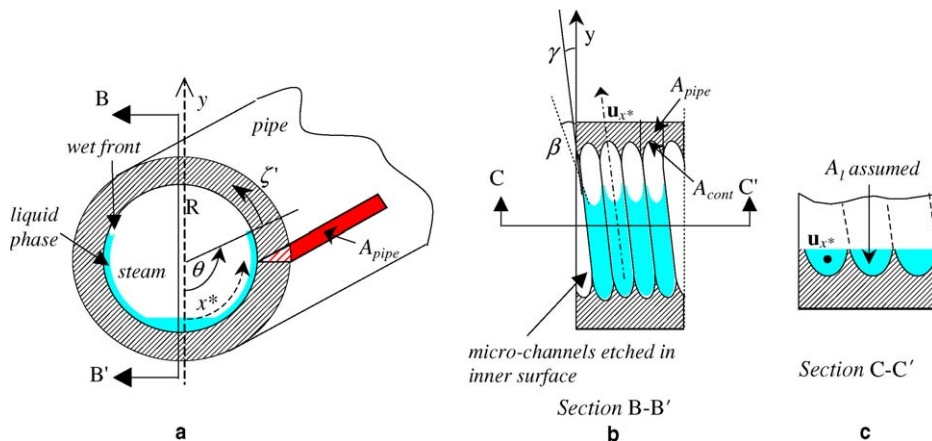


Fig. 1. Illustration of variables in a microgrooved pipe.

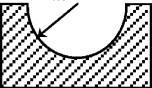
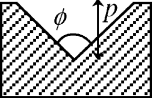
of the micro-channel and A_{cont} is the surface in contact with the liquid layer (Fig. 1(b)); A_1 is the wetted cross section of the micro-channel (Fig. 1(c)).

The following assumptions were made for Eq. (2):

- the thickness of the liquid layer flowing in the micro-channel is negligible compared to the inner radius of the pipe, R , and has a constant wetted cross section, A_1 , i.e., $m_1 = A_1 \rho_l \frac{R\theta}{\cos \gamma}$ and $v_1 = \frac{R}{\cos \gamma} \frac{d\theta}{dt}$, where t is the time;
- the liquid layer is isothermal, so its internal friction is negligible (Prasad et al., 1992);
- the flow in the micro-channel is laminar and Newtonian.

Micro-channels are usually etched by a milling machine, so, theoretically, the cross section is always triangular. Nevertheless, the cutting edge of the blades is not perfect, which implies that, depending on the depth of the grooves, micro-channels may have not only a triangular cross section, characterized by groove depth, p , and apex angle, ϕ , but also a semicircular cross section, characterized by groove radius, r_m (Table 1). The geometry assumed for the micro-channel determines parameters r_H , A_{cont} and A_1 in Eq. (2) and Table 1. The effective capillary radius, r_c , is defined as the characteristic length governing the flow rate through the capillary system and may be considered to be twice the hydraulic radius, i.e., $r_c = 2r_H$, in the same way as common hydraulics practice. As this is commonly assumed when studying capillarity in porous media (Dullien, 1992), its validity for micro-channels is reinforced by the experimental results of Peng et al. (1993), who measured the effective capillary radius of a pipe sample with V-shaped grooves, 0.635×10^{-3} m wide and a 60°

Table 1
Characteristics parameters of micro-channels depending on their geometry and configuration

Micro-channels	r_H	r_c	A_1	A_{cont}	A_{pipe}
 Semicircular	$\frac{1}{2}r_m$	r_m	$\frac{1}{2}\pi r_m^2$	$\pi r_m R \theta \cos \gamma$	$2r_m \delta - \frac{1}{2}\pi r_m^2 \underset{r_m \ll \delta}{\cong} 2r_m \delta$
 Triangular $\forall \phi$	$\frac{1}{2}p \text{sen}(\phi/2)$	$p \text{sen}(\phi/2)$	$p^2 \text{tang}(\phi/2)$	$\frac{2pR\theta}{\cos(\phi/2)} \cos \gamma$	$(2p\delta - p^2) \text{tang}(\phi/2) \underset{p \ll \delta}{\cong} 2p\delta \text{tang}(\phi/2)$
$\phi = 60^\circ$	$\frac{1}{4}p$	$\frac{1}{2}p$	$\frac{p^2}{\sqrt{3}}$	$\frac{4}{\sqrt{3}}pR\theta \cos \gamma$	$\cong \frac{2}{\sqrt{3}}p\delta$

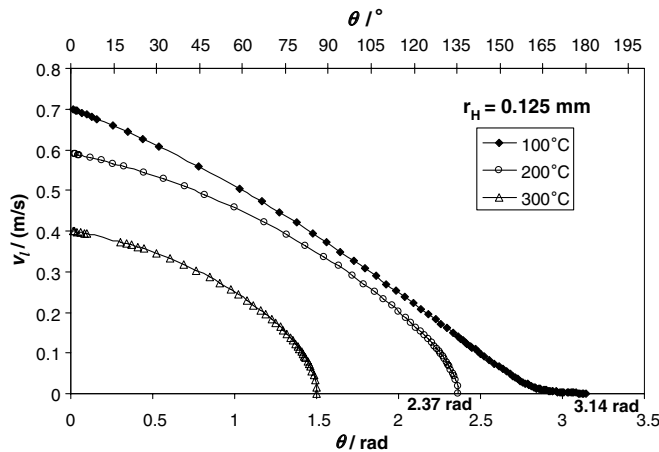


Fig. 2. Liquid front velocity in absence of heat flux, v_l , as function of liquid front positions, θ (solutions of Eq. (2)); considering a pipe with a 50×10^{-3} m inner diameter with vertical micro-channels (0.125×10^{-3} m hydraulic radius of micro-channels, r_H), at different operating temperatures.

apex angle, using three different working fluids. They obtained an effective capillary radius of 0.26×10^{-3} m with a variation of less than 1%. For their grooves, the hydraulic radius is 0.137×10^{-3} m and the effective capillary radius, obtained assuming $r_c = 2r_H$, is 0.27×10^{-3} m, only 4% lower than the one found experimentally.

Eq. (2) can be applied to any given micro-channel configuration/geometry. For example, for a vertical ($\gamma = 0^\circ$), semicircular micro-channel (with radius r_m), it is

$$\frac{dv_1}{d\theta} = \frac{1}{\rho_1 \theta v_1} \left(\frac{2\sigma \cos \beta}{r_m} - \rho_1 g R (1 - \cos \theta) - \mu_1 \frac{4v_1 R \theta}{r_m^2} - v_1^2 \rho_1 \right), \quad (3)$$

which is the expression proposed by Peng et al. (1993).

Eqs. (2) and (3) can only be solved numerically. In Fig. 2 the v_1 -solutions of Eq. (2) are shown at different operating temperatures for a pipe with a 50×10^{-3} m inner diameter and vertical micro-channels with a hydraulic radius of 0.125×10^{-3} m. The contact angle, β , is assumed always equal to zero. The liquid front velocity, v_1 , is maximum when the liquid layer starts rising, i.e., for low θ values. As the liquid layer becomes longer (higher θ values), the velocity diminishes until an angular position such that it is zero. This angular position determines the maximum advance of the liquid front under fixed conditions, and may be referred to as the maximum ‘dynamic’ liquid front position. This means that, in Fig. 2 for example, at 200 °C, the maximum dynamic liquid front is at 2.37 rad ($\sim 135.8^\circ$). As mentioned above, at this position, the liquid front velocity is zero, which means that gravitational forces are compensating capillary pressure forces (static balance of forces), i.e.,

$$(\text{gravitational forces})_{x^*} = (\text{capillary driving forces}) \iff -\rho_1 g A_1 R (1 - \cos \theta) \cos \gamma = \frac{2\sigma \cos \beta}{r_c} A_1. \quad (4)$$

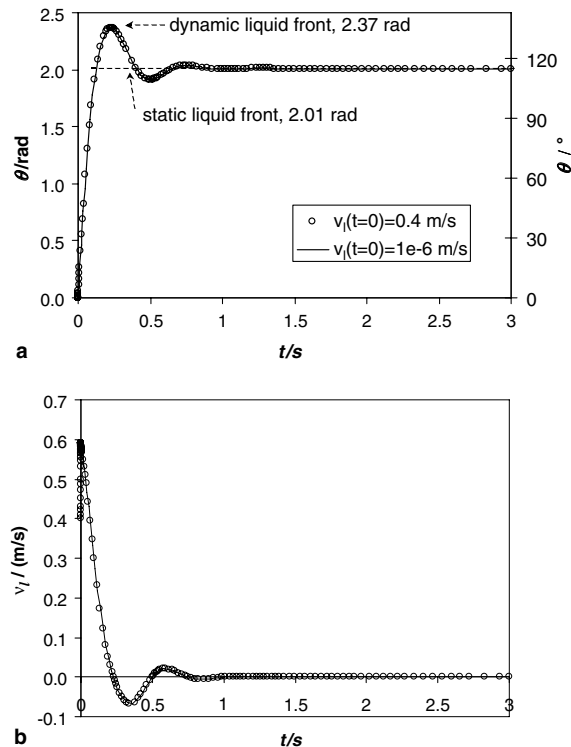


Fig. 3. (a) Liquid front velocity in absence of heat flux, v_1 , and (b) liquid front positions, θ , as functions of time, t (solutions of Eq. (5)); considering a pipe with a 50×10^{-3} m inner diameter with vertical micro-channels (0.125×10^{-3} m hydraulic radius of micro-channels, r_H), at an operating temperature of 200 °C.

When Eq. (4) is used to determine the maximum position of the liquid front (called the ‘static’ liquid front) the results are lower than the dynamic liquid front calculated above. Thus, at 200 °C the static liquid front is 2.01 rad (~115.2°). To understand this apparent inconsistency Eq. (2) must be reformulated using time, t , as independent variable instead of the liquid front position, θ , and the definition of the liquid front velocity considered, i.e., to solve the following equation:

$$\begin{cases} \frac{d\theta}{dt} = \frac{\cos \gamma}{R} v_1, \\ \frac{\theta R}{\cos \gamma} \frac{dv_1}{dt} = \frac{2\sigma \cos \beta}{\rho_1 r_c} - gR \cos \gamma (1 - \cos \theta) - \mu_1 \frac{v_1}{r_c/2} \frac{A_{\text{cont}}}{A_1 \rho_1} - v_1^2, \end{cases} \quad (5)$$

without forgetting that A_{cont} depends on θ (Table 1).

Solutions $\theta = \theta(t)$ and $v_1 = v_1(t)$ found with Eq. (5) for the example mentioned are shown in Fig. 3. These solutions were obtained using Matlab code ode15s, a quasi-constant step size implementation of the numerical differentiation formulas in terms of backward differences (Shampine and Reichelt, 1997). To avoid additional errors, the analytical formula of the Jacobian of Eq. (5) has been entered in the code. It can be seen in Fig. 3(a) how the liquid front passes the static limit, 2.01 rad, with certain inertia, up to the maximum dynamic liquid front (2.37 rad). This point is unstable and becomes, with some minimal oscillation, the static limit. In less than 1 s the liquid front stabilizes at the static limit. In the figure for the liquid front velocity (Fig. 3(b)) the negative values have to be interpreted as a change in flow direction. Representing $v_1 = v_1(\theta)$ parametrically (Fig. 4), this oscillation is translated into loops around the static limit. The first part of the curve, i.e., until the velocity first cuts the θ axis, is identical to the one obtained by solving Eq. (2) (Fig. 2).

To solve Eq. (5), two initial conditions have to be imposed: $\theta(t=0)$ and $v_1(t=0)$. While the starting condition is known for the position of the liquid front, $\theta(t=0) = 0$, the starting condition for its velocity is arbitrary. Figs. 3 and 4 show solutions with two different starting conditions for v_1 : $v_1(t=0) = 10^{-6}$ m/s and $v_1(t=0) = 0.4$ m/s. These figures reveal that this initial condition is not critical, as the v_1 profiles soon join in the same curve.

Thus, the results obtained with the static and dynamic force balances are coherent: the dynamic limit tends towards the static limit. Bearing in mind the time of response of this kind of system (less than 1 s in the case mentioned) this means that, with no external heat flux, the static force balance is good enough to determine what portion of the inner surface of a pipe with micro-channels stays wet.

2.2. With heat flux

Let us now suppose that heating power Q (W) is used to evaporate a certain mass of liquid, $\dot{m}_{\text{evaporated}}$, flowing through a micro-channel,

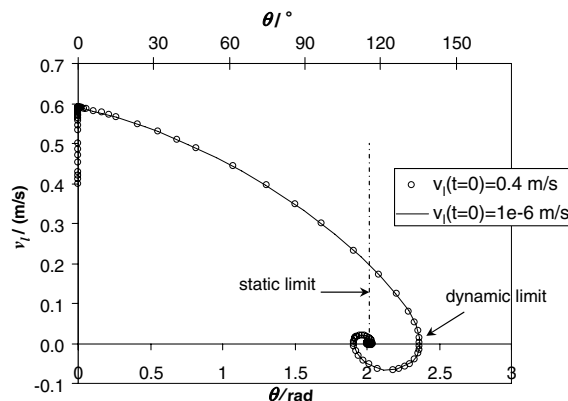


Fig. 4. Parametric solutions of the liquid front velocity in absence of heat flux, v_1 , as a function of the liquid front position, θ (Eq. (5)) assuming two different initial conditions for v_1 ; and considering a pipe with a 50×10^{-3} m inner diameter with vertical micro-channels (0.125×10^{-3} m hydraulic radius of micro-channels, r_H), at an operating temperature of 200 °C.

$$Q = \dot{m}_{\text{evaporated}} \lambda, \quad (6)$$

where λ is the latent heat of evaporation. Two approximations to the maximum useful external heat flux that can be applied to the outer pipe surface, q_{max} , are possible.

One approximation is to limit the maximum heat flux to that which evaporates all the liquid flowing in the capillary system, i.e., in the micro-channel. This approximation, followed by Malysenko (1996) for porous coatings, means that the evaporated liquid mass is given by

$$\dot{m}_{\text{evaporated}} = v_1 A_1 \rho_1, \quad (7)$$

so the heat power for that process is $Q = v_1 A_1 \rho_1 \lambda$ or in terms of heat flux, $q_{\text{max}} = \frac{Q}{S_{\text{pipe}}^{\text{ext}}} = \frac{v_1 A_1 \rho_1 \lambda}{S_{\text{pipe}}^{\text{ext}}}$ where $S_{\text{pipe}}^{\text{ext}}$ is the external surface of the pipe.

The other approximation consists of limiting the heat flux to that which keeps some liquid in the micro-channel flowing with a new liquid front velocity v'_1 . This approximation was followed by Peng et al. (1993) and Peng and Peterson (1991) for vertical and semicircular micro-channels, and can be expressed as

$$\dot{m}_{\text{evaporated}} = (v_1 - v'_1) \rho_1 A_1 \quad \text{so} \quad Q = (v_1 - v'_1) \rho_1 A_1 \lambda. \quad (8)$$

With no external heat flux, the inner surface of the pipe is at the temperature given by the saturation conditions of the bulk two-phase flow, T_{sat} . When external heat flux, q , is applied, this inner surface rises to a temperature higher than the liquid saturation temperature and cools down as the liquid flows within the micro-channels. Assuming that heat is transferred at an angle from the dry to the wet zone of the pipe, that convective and radiation heat transfers between pipe and steam are negligible and that groove depth is much smaller than pipe thickness, the temperature of the inner surface of the pipe, T_{pipe} , is given by (Rojas, 2003)

$$T_{\text{pipe}} = T_{\text{sat}} + \frac{q}{\delta \rho_{\text{pipe}} c_{p,\text{pipe}}} \frac{R \zeta'}{v'_1}, \quad (9)$$

where k_{pipe} , ρ_{pipe} , $c_{p,\text{pipe}}$ and δ are the conductivity, density, specific heat at constant pressure and thickness of the pipe, respectively, and ζ' is the angular relative coordinate ($v'_1 = \frac{R d\zeta'}{dr}$).

This pipe temperature profile gives the heat power conduction at the wetting front:

$$Q = A_{\text{pipe}} k_{\text{pipe}} \frac{1}{R} \left. \frac{dT_{\text{pipe}}}{d\zeta'} \right|_{\zeta'=0} = A_{\text{pipe}} k_{\text{pipe}} \frac{1}{R} \left(\frac{q}{\delta \rho_{\text{pipe}} c_{p,\text{pipe}}} \frac{R}{v'_1} \right), \quad (10)$$

where A_{pipe} is the radial section of the pipe (Fig. 1(a) and (b)). Imposing the simplification that vaporization occurs only at the wetting front due to such heat power, Eqs. (10) and (8) must be equated. Solution v'_1 of this equation contains a square root that defines a maximum value for q (called q_{max}),

$$q_{\text{max}} = \frac{\delta \rho_1 \lambda}{4 \alpha_{\text{pipe}}} \frac{A_1}{A_{\text{pipe}}} v_1^2, \quad (11)$$

where α_{pipe} is the thermal diffusivity of the pipe. This equation also allows the maximum wetting-front position to be calculated for a fixed power supply (because of dependence of v_1 on θ), whenever this power supply is lower than the critical heat flux, i.e., whenever there is a liquid film on the surface.

Detailing A_1 and A_{pipe} in Eq. (11) for vertical, semicircular (with radius r_m) micro-channels (Table 1), yields:

$$q_{\text{max}} = \frac{\pi r_m \rho_1 \lambda}{16 \alpha_{\text{pipe}}} v_1^2, \quad (12)$$

which is the expression presented by Peng et al. (1993).

It should be mentioned that this last approximation not only relates maximum external heat flux to heat power employed to evaporate the liquid flowing in the micro-channel as in the first approximation, but also to the ability of the pipe to transmit external flux by conduction (through the thermal diffusivity term) and to the ability of the liquid film to cool the pipe (through the liquid-film velocity term in absence of heat flux). The maximum external heat flux is, firstly, limited by the liquid-film velocity profile, v_1 , and consequently by the maximum liquid front position determined by this velocity. As seen above, depending on whether the system stabilizes or not, we can speak of maximum static or dynamic liquid front positions. When external heat flux is

applied, we cannot assure that the liquid film stabilizes at the static limit, as some of it is continuously being evaporated, but the maximum liquid front position is definitely within the range determined by the static and dynamic limits.

3. Experimental study

Two carbon steel pipe samples, M#1 and M#2, with inner/outer diameters of $52 \times 10^{-3}/70 \times 10^{-3}$ m and a length of 10^{-1} m, were tested. The main geometrical characteristics of the micro-channels etched in the inner surface of the samples are shown in Table 2. Each sample was partially immersed in water in an autoclave (Fig. 5), which is a closed thermal mass system with operating temperature controllable during experiments. The external heat flux is provided by a heating element coiled around the outside of the sample (Fig. 5(6)). The methodology proposed by Rojas (2003) and Rojas and de Andrés (2004) was used to quantify the liquid front positions on the inner and outer surfaces of each sample. This methodology uses a unidimensional temperature profile measured inside the sample, which is interpreted with the aid of an effective heat transfer coefficient. Six K-type thermocouples (T1–T6 in Fig. 5(6)), at different angular positions, give the required experimental temperature profile. Experiments were carried out at different saturation temperatures, from 100 °C to 266 °C, and different external power supplies, from 137 W to 1186 W. Water mass was the minimum necessary to reach the lower point on the inner surface of the sample at ambient temperature (Point A in Fig. 5). The level up to which the sample is submerged varies due to thermal expansion of the water and in each experiment is determined by operating temperature, T_{sat} . The experimental results shown are corrected for this level.

The experimental conditions (temperature and external power supply) for both samples are shown in Table 3. The experimental ranges of the liquid front positions are listed in Column 4. The theoretical static and dynamic levels to which the liquid film rises for these working conditions are shown in Columns 5 and 6, respectively. They have been calculated by finding the point where the experimental heat flux intersects with

Table 2
Characteristics of the micro-channels in the test samples: p is their depth and γ is their inclination

Sample	p (mm)	Thread (mm)	Pitch	γ (°)
M#1	0.78	–	–	0
M#2	0.79	28.7	31	10

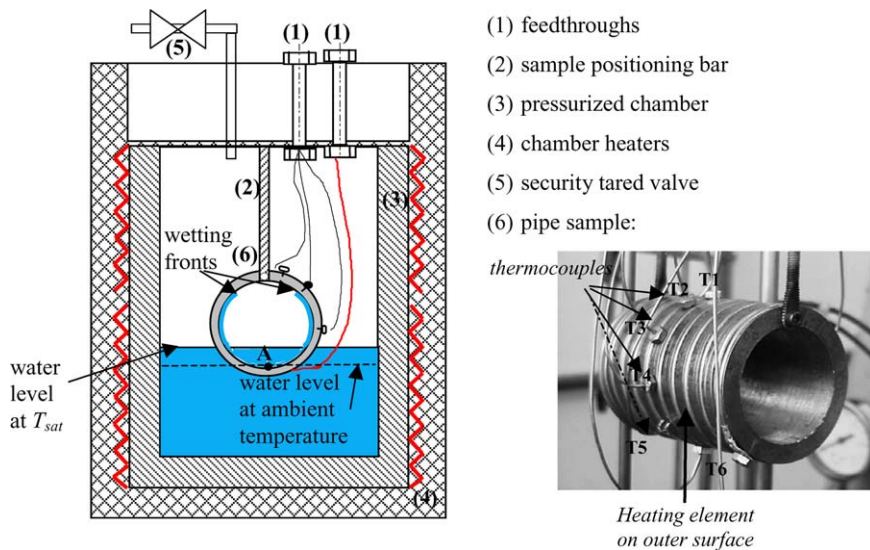


Fig. 5. Schematic diagram of measuring set-up.

Table 3

Experimental and theoretical results for different operating conditions. T_{sat} is the operating temperature and P_{ext} is the external power supply

Sample	T_{sat} (°C)	P_{ext} (W)	Liquid front position on inner surface of samples			
			Experimental	Theoretical		Comments
				Static	Dynamic	
M#1	100	137 ± 5	80–126°	120	134	$\beta = 66.4^\circ$
				111	123	$\beta = 72.4^\circ$
	125	264 ± 8	90–125°	111	126	$\beta = 66.4^\circ$
				103	116	$\beta = 72.5^\circ$
	150	260 ± 7	160–180°	159	180	$\beta = 0^\circ$
642 ± 12				159	180	$\beta = 0^\circ$
266	1186 ± 15	180°	172	180	$\beta = 0^\circ$	
M#2	100	137 ± 5	90–125°	111	123	$\beta = 72.5^\circ$
				101	111	$\beta = 78.5^\circ$
	120	264 ± 8	124–160°	122	137	$\beta = 66.4^\circ$
				130	147	$\beta = 60.0^\circ$
				159	180	$\beta = 0^\circ$
	187	748 ± 12	70–126 ^{oa}	–	–	
	200	515 ± 10	180°	168	180	$\beta = 0^\circ$
				742 ± 12	168	180
	220	860 ± 13	180°	171	180	$\beta = 0^\circ$
1126 ± 15				–	–	
250	1126 ± 15	80–126 ^{oa}	–	–		

^a Water level at corresponding operating temperature.

the limiting value given by Eq. (11). This intersection depends on the contact angle by Eq. (5). Contact angles, β , considered and introduced in the calculations are the ones which fit experimental to theoretical results (they are in *Comments* column in Table 3).

When the operating temperature is below 150 °C, several theoretical solutions can be found which agree with the experimental results. These solutions differ slightly in the contact angle employed in Eq. (5). Thus, for sample M#1, the experimental results can be predicted by the model presented here if contact angle, β , is around 70° at operating temperatures under 150 °C and 0° at higher temperatures. Apart from surface roughness and cleanness and phase purity involved, the contact angle depends on the operating temperature, decreasing in most cases with increasing temperatures (Carey, 1992; Olek et al., 1988). Bernardin et al. (1997) found that the contact angle of water over polished aluminium hardly diminishes up to a set operating temperature, where it rapidly drops to zero. For the case studied by Bernardin et al., this temperature is around 120 °C. Although these results cannot be directly applied to the samples studied here, the behaviour deduced from experimental results seems to be quite similar: the contact angle for water on carbon steel is around 70° up to an operating temperature between 120 °C and 150 °C, quickly dropping to zero at higher temperatures. As expected, this behaviour is also detected in the experimental results for sample M#2. The contact angles are slightly different, but in the same range. These small differences can be attributed to the fact that the contact angles are not measured directly, but are the result of applying the theoretical model, and to have the surfaces of the two samples not exactly in the same state. Observations after testing show that the inner surface of sample M#2 is rougher than the one in M#1 (Fig. 6). This roughness is due to randomly distributed rust spots on the inner surface.

The experimental liquid front position on the inner surface of sample M#2 is the same as on the outer surface at 187 °C/748 W and 250 °C/1126 W. This means that there is no significant capillary rise or that, if there were, it would not withstand the external heat flux applied. As sample M#2 is quite similar to sample M#1 in terms of material and micro-channel depth (the main difference is that in M#2 the micro-channels are not vertical but inclined 10° with respect to the vertical), this result is surprising at first. As sputtering can play an important role in reducing the ability of a liquid layer to drain heat, its effect has been quantified using the model developed by Peng et al. (1993) and Peng and Peterson (1991). According to their model, to validate the experimental results at these conditions, it would be necessary that 0.018% of the liquid film vaporized, forcing the rest of the liquid film to be sputtered away. Although there is no doubt that sputtering can signif-

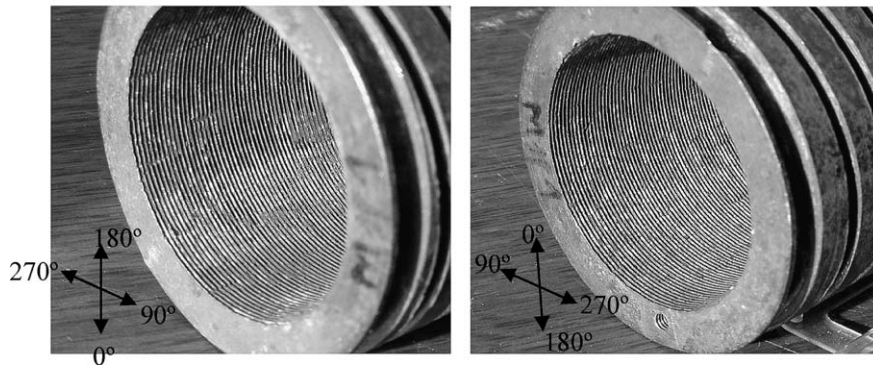
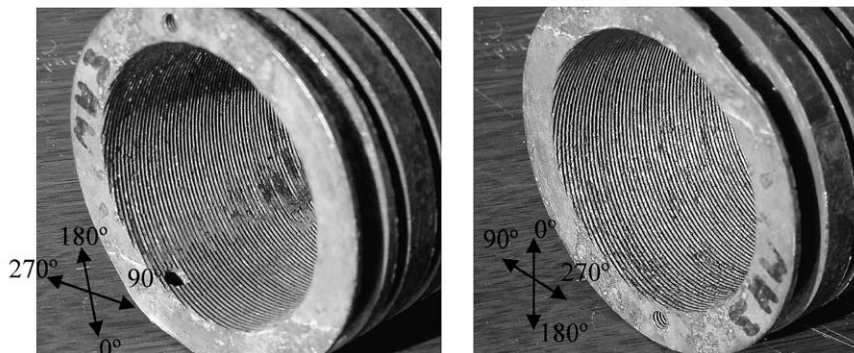
M#1: ‘clean’ micro-channels**M#2:** rust spots randomly distributed in micro-channels

Fig. 6. Photographs of samples M#1 and M#2 after testing.

icantly diminish the maximum applicable heat flux, it is hard to believe that the steam of only 0.018% of the liquid film, is sufficient for the rest of the water to be eliminated from the micro-channel. We suggest the possibility that at the above experimental conditions, the critical heat flux has already been reached, so the model presented here cannot predict the results. This means the critical heat flux at 187 °C is lower than $3.4 \times 10^4 \text{ W/m}^2$ (748 W) and at 250 °C is lower than $5.12 \times 10^4 \text{ W/m}^2$ (1126 W). These values are quite a bit lower than those obtained using commonly used correlations for water in pool boiling (Costa Novella, 1986; for example), but in fairly good agreement with the results of Patten and Turmeau (1970) on bubble formation in liquid-film layers less than $5 \times 10^{-3} \text{ m}$ thick. In their study it was found that the critical heat flux for such thin liquid films is much lower than for thick films, and thus for most correlations given in the literature.

The reason why this behaviour is found only on sample M#2 and not on sample M#1 is that, as mentioned above, there are small rust spots on the inner surface of sample M#2, which could be also responsible for the small difference in contact angle. Rust particles can be active nucleation sites, so bubble formation is promoted and the transition to boiling is faster than when there is no oxidation, i.e., in sample M#1. The M#2 facility for forming bubbles and thereby coming to a stable boil can also be detected in the experimental times necessary to achieve stable temperatures, which were much higher for M#1 than for M#2. For example, at an operating temperature of around 186 °C and external power of 748 W, after a little less than 2 h, temperatures in sample M#1 remained unstable, while for sample M#2 it took less than 45 min to have a stable pipe temperature profile.

4. Conclusions

A theoretical and experimental thermohydraulic study of fluids in open micro-channels etched in the inner surface of externally heated horizontal pipes containing two-phase flow has been performed. The main goal

was development of a predictive model for the liquid–steam–solid front position and the maximum external heat flux able to keep the same portion of pipe wet as when there is no heat flux.

The balance of dynamic forces acting on the liquid layer flowing in a micro-channel with any configuration and characteristics has been considered. As the dynamic solution rapidly converges at the same point, as does the static balance, when there is no external heat flux, the static balance is sufficient to predict the position of the liquid front in the micro-channel. Pipes with micro-channels in the inner surface are mostly used for enhancing heat transfer, so external heat flux should be considered the most realistic situation. In this case, the front position reached by the liquid layer in the micro-channels is in the range given by the static and dynamic solutions. These solutions make sense whenever the critical heat flux has not already been reached.

Tests were performed with samples of steel pipes with two different types of micro-channels, with saturated water at temperatures ranging from 100 °C to 250 °C and external heating power from 137 W to 1186 W. Experimental and theoretical results are in fairly good agreement, assuming that the contact angle for water–steam–steel interface is around 70° when the operating temperature is below 150 °C and drops to zero over this limit.

If the proposed model is accepted as valid, some of the experimental results imply that the critical heat flux for liquid films depends on the thickness of the liquid layer and the condition of the solid surface in contact with it. The thinner the liquid layer is, the lower the critical heat flux. On the other hand, oxidation can create new nucleating centres, which promote bubbling, thereby lowering critical heat flux. This could strongly limit the applicability of this kind of capillary system to heat transfer enhancement.

References

- Bernardin, J.D., Mudawar, I., Walsh, C.B., Franses, E.I., 1997. Contact angle temperature dependence for water droplets on practical aluminum surfaces. *Int. J. Heat Mass Transfer* 40, 1017–1033.
- Carey, V.P., 1992. *Liquid–vapor Phase-change Phenomena. An Introduction to the Thermophysics of Vaporization and Condensation Processes in Heat Transfer Equipment*. Hemisphere Publishing Co.
- Costa Novella, E., 1986. *Transmisión de calor*. Ingeniería Química, vol. 4. Alhambra Universidad, Spain.
- Dullien, F.A.L., 1992. *Porous Media. Fluid Transport and Pore Structure*, second ed. Academic Press, Inc, San Diego, CA, pp. 397–415.
- Honda, H., Wang, Y.S., 2004. Theoretical study of evaporation heat transfer in horizontal microfin tubes: stratified flow model. *Int. J. Heat Mass Transfer* 47, 3971–3983.
- Malyshenko, S.P., 1996. Boiling phenomena in direct steam generators with porous coatings. Interim Report, IVTAN, Moscow.
- Olek, S., Zvirin, Y., Elias, L., 1988. The relation between the rewetting temperature and the liquid–solid contact angle. *Int. J. Heat Mass Transfer* 1, 898–902.
- Patten, T.D., Turmeau, W.A., 1970. Some characteristics of boiling in thin liquid layers. In: 4th Int. Heat Transfer Conference, Paper B2.10.
- Peles, Y.P., Yarin, L.P., Hetsroni, G., 2001. Steady and unsteady flow in a heated micro-channels. *Int. J. Multiphase Flow* 28, 1589–1616.
- Peng, X.F., Peterson, G.P., 1991. Analysis of rewetting for surface tension induced flow. *Phase Change Heat Transfer*, HTD-vol. 159. ASME, pp. 69–74.
- Peng, X.F., Peterson, G.P., Wang, B.X., 1992. On the wetting mechanism of liquid flow on hot surfaces. *Int. J. Heat Mass Transfer* 35, 1615–1624.
- Peng, X.F., Peterson, G.P., Lu, X.J., 1993. Analysis rewetting in circular channels with internal grooves. *J. Thermophysics Heat Transfer* 7, 334–339.
- Prasad, V., Lauriat, G., Kladias, N., 1992. Non-Darcy natural convection in a vertical porous cavity. In: Quintard, M., Todorovic, M. (Eds.), *Heat and Mass Transfer in Porous Media*. Elsevier Science Publishers B.V., Amsterdam, pp. 293–314.
- Rojas, M.E., 2003. *Mejora de la transferencia de calor en flujo horizontal bifásico. Aplicación a colectores solares cilindro-parabólicos*. Ph.D. Thesis, Universidad Complutense, Madrid, Spain.
- Rojas, M.E., de Andrés, M.C., 2004. A new methodology for experimental determination of liquid–gas interface positions on a heated solid. *Int. J. Heat Mass Transfer* 47, 5085–5093.
- Scheidegger, A., 1957. *The physics of flow through porous media*, third ed. University of Toronto Press, Toronto, pp. 113–120.
- Shampine, L.F., Reichelt, M.W., 1997. The MATLAB ODE suite. *SIAM J. Sci. Comput.* 18, 1–22.
- Webb, R.L., 1994. *Principles of Enhanced Heat Transfer*. John Wiley & Sons Inc., New York.
- Yoshida, S., Matsunaga, T., Hong, H.P., Nishikawa, K., 1987. Heat transfer to refrigerants in horizontal evaporator-tubes with internal spiral grooves. In: Marto, P.J. (Ed.), *Proc. 1987 ASME-SSME Thermal Eng. Joint Conf.*, vol. 5. pp. 165–172.
- Yun, R., Kim, Y., Seo, K., Kim, H.Y., 2002. A generalized correlation for evaporation heat transfer of refrigerants in micro-fin tubes. *Int. J. Heat Mass Transfer* 45, 2003–2010.